IEEE Access
Multidisciplinary | Rapid Review | Open Access Journal

Received December 3, 2020, accepted December 14, 2020, date of publication December 21, 2020,
date of current version December 31, 2020.

Digital Object Identifier 10.1109/ACCESS.2020.3045933

Multiple Sensor Linear Multi-Target Integrated Probabilistic Data Association for Ultra-Wide Band Radar

MINHO SHIN AND HUNGSUN SON, (Member, IEEE)
Department of Mechanical Engineering, Ulsan National Institute of Science and Technology, Ulsan 44919, South Korea

Corresponding author: Hungsun Son (hson@unist.ac.kr)

This work was supported in part by the Future Innovation Research Funds through the Ulsan National Institute of Science and Technology (UNIST) under Grant 1.200034.01, in part by the Development of Drone System for Ship and Marine Mission through the Civil Military Technology Cooperation Center under Grant 2.180832.01, in part by the National Research Foundation of Korea (NRF) grant funded by the Korea Government (MSIT) under Grant 2020R1F1A1075857, and in part by the Basic Science Research Program through the National Research Foundation of Korea (NRF) funded by the Ministry of Education under Grant 2020R1A6A1A03040570.

ABSTRACT Ultra-Wide Band (UWB) radar has a number of advantages of resolving multipath, exceptional spatial resolution, and ranging performance. However, several difficulties are confronted for multiple target tracking using UWB radars such as clutter signals which contaminate target signals, and unidentified number and behavior of the targets. Hence, this paper presents to develop a multiple moving target tracking algorithm, consisting of preprocessing and multiple target tracking steps. In the preprocessing step, static clutter reduction and constant false alarm rate (CFAR) detection extract the target candidate range measurements from each UWB radar. Then, two multiple target tracking (MTT) steps are developed: range- based MTT and position-based MTT. The range-based MTT is mainly based on existing linear multi-target integrated probabilistic data association (LM-IPDA) from each UWB radar measurement. Then the outputs of each LM-IPDA are gathered in the positioning center to estimate the position of multiple targets. On the other hands, the position-based MTT is based on multiple sensor LM-IPDA (msLM-IPDA) as an accurate target tracking method for various uncertainties by improving the probabilistic model of LM-IPDA. The tracking performance of two MTT methods is investigated with both numerical simulation and experiments.

INDEX TERMS UWB, IR-UWB radar, multiple target tracking, probabilistic data association, LM-IPDA, localization.

I. INTRODUCTION

Recently, a number of applications require information on the target position for rescue, surveillance, and monitoring, etc. In particular, passive approach systems such as sound navigation and ranging (Sonar) and light detection and ranging (Lidar), have advantages of standalone and low cost because of no supplementary device. However, most passive approach systems are often degraded by environmental interferences. On the contrary, active approach systems such as Ultra-Wide Band (UWB) radar has a number of advantages of resolving multipath, mitigating obstacles [3], etc. Impulse Radio UWB (IR-UWB) technology offers an exceptional spatial resolution and ranging performance because of the transmission of a few nanosecond duration pulses. Moreover, it provides low power consumption and through-wall detectability [4]. The UWB radar has gained increasing attention in a number of applications such as vital sign detection [5], through-wall target tracking [6], [7], and gesture recognition [8]. However, a number of complexities to track multiple targets are confronted due to the unidentified number and behavior of targets. Moreover, clutter signals from undesired sources such as moving obstacles, thermal noises, or multipath effects contaminate the target signals, so that it becomes difficult to identify and track the true target measurement.

Data association algorithms deal with measurement (belongs to target and clutter) to track association where each track is initialized based on a two-point initialization technique [9]. Single target tracking (STT) algorithms such as Probabilistic Data Association (PDA) [9] and Integrated

The associate editor coordinating the review of this manuscript and approving it for publication was Pinjia Zhang.

PDA (IPDA) [10] do not deal with a possibility of a measurement that may have originated from a target not being followed by other tracks. Thus, STT algorithms cannot be applied for multi-target tracking in the UWB radar system. On the contrary, multi-target tracking (MTT) algorithms such as Joint PDA (JPDA) [11] and Joint IPDA (JIPDA) [12] involve joint data association procedure. The joint data association generates all feasible joint (shared) measurement-to-track association postulates being followed by other tracks. The number of feasible joint measurement postulates grows combinatorically with the number of tracks and the number of measurements involved. Hence, it is difficult to apply a joint data association algorithm in a real-time tracking system. A linear multi-target (LM) approach to overcome the difficulties has been developed in [13] which enables the tracking system to avoid entire process of joint data associating, allowing the tracking system to function as a single target tracker. The LM algorithm, for example, LM-IPDA [13] modifies the clutter measurement with other targets (foreign targets) measurement being followed by other tracks. Thus, when updating one track, other targets being considered as a modified clutter measurement. Therefore, the LM is beneficial to apply in the real-time tracking system due to its low computational time consumption and accuracy in estimation.

In case of multi-static structure UWB radar systems (or other ToA based system), range measurements from each UWB radar are used to estimate target positions by a multilateration. The probabilistic model depends on whether the state of the MTT is range or position. In the case of range-based MTT, the LM-IPDA is applied to track the range between the UWB radar and targets using target candidate range measurement in each UWB radar. Then the tracked ranges from each UWB radar are gathered in the positioning center to estimate positions of the multiple targets by multilateration. For position-based MTT, on the other hand, target candidate range measurements from each UWB radar are gathered in the LM-IPDA like MTT algorithm as measurements. The algorithm tracks the positions of multiple targets based on the relationship between the state and measurements. However, the existing LM-IPDA cannot be applied to the position-based tracking since the LM-IPDA is a single-sensor MTT algorithm. Therefore, multiple sensor LM-IPDA (msLM-IPDA) is proposed for robust and accurate tracking performance.

In [14], a single target detection algorithm in two-dimension is developed by using Kalman filter (KF) static clutter reduction and CLEAN detection algorithm. Extended KF (EKF) and Unscented KF (UKF) are used for target tracking. The results of accuracy as root mean square error (RMSE) are 0.24 and 0.23 meters, respectively. In [15] and [16], multi-target positioning and respiration detection algorithm using three UWB radars is developed to detect positions and respiration signals of multiple static targets. Firstly, the respiration signals are detected by signal processing in frequency domain for reducing false alarms. Then, target detection is performed by a maximum likelihood method, which explores all possible combinations for data association. The positioning accuracy in three static target case is around 0.3 meters, but the accuracy varies according to the number of targets, positions of targets, and other parameters. In [17], the MTT algorithm based on the Gaussian mixture probability hypothesis density filter is developed. In this algorithm, four UWB radars are used in a distributed multi-static structure, and two targets are used for verifying the performance of the MTT algorithm with 0.25 meter accuracy.

This paper develops a novel multi-target tracking system based on multiple sensor linear multi-target integrated probabilistic data association (msLM-IPDA) using bistatic UWB radar system. The MTT algorithm is designed as two steps: preprocessing and multiple target tracking step. First in a preprocessing step, KF static clutter reduction and cell averaging constant false alarm rate (CA-CFAR) detection methods are utilized to extract target candidates. Then, two different MTT algorithms are investigated to track multiple targets with two probability models. One is a range-based MTT utilizing the existing LM-IPDA. To apply the LM-IPDA to the range-based MTT, multiple LM-IPDA as the number of UWB radar should be applied. The other is a position-based MTT algorithm referred here to as msLM-IPDA. The tracking performance of the msLM-IPDA is demonstrated in both numerical simulation and experiments with UWB radars. The results show the msLM-IPDA is able to track multiple targets accurately and robustly in practical scenarios.

II. MULTI-TARGET TRACKING ALGORITHM

Fig. 1 shows the overall flowchart of both range-and position-based target tracking algorithms using UWB radars. The algorithm is mainly divided into two steps: preprocessing and multiple target tracking step. The UWB radars transmit signals to receive the reflected signals from targets as well as clutters in each scan. In a clutter environment, the target candidate signals are detected by the preprocessing step consisting of static clutter reduction and CFAR detection. Once the ranges of the targets from the UWB radars are computed, the position of the targets can be estimated by multilateration and tracked by either range- or position-based MTT algorithm.

Suppose that the UWB radar receives reflected signals and stores them in each frame, typically called radar scan with m samples. The radar scan stores information of signal strength with respect to the sample number denoted as $\mathbf{r}[m]$. In addition, the radar scan includes not only signals from the target, $\mathbf{r}_t[m]$, but also signals from various clutters, $\mathbf{r}_c[m]$, and additive noises, $\mathbf{r}_N[m]$, as expressed in (1). Therefore, it is essential to extract target signals from the radar scan for accurate positioning computation.

$$r[m] = r_t[m] + r_c[m] + r_N[m] \tag{1}$$

A. PREPROCESSING STEP

The static clutter reduction method using the KF is able to track the signals from static clutter and extracts signals from moving targets in each radar scan in (1). The signals

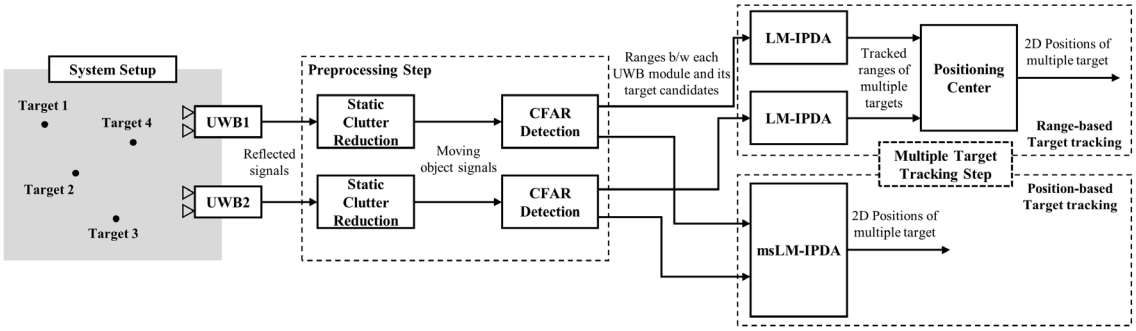

FIGURE 1. Overall flowchart of multi-target tracking algorithms.

from stationary objects such as background walls generate stationary amplitude and propagation delay. The state and measurement equations can be expressed in (2).

$$\begin{aligned} \mathbf{X}_k^{CR} &= \mathbf{F}\mathbf{X}_{k-1}^{CR} + \mathbf{w}_{k-1}^{CR} \\ \mathbf{Z}_k^{CR} &= \mathbf{H}\mathbf{X}_k^{CR} + \mathbf{v}_k^{CR} \end{aligned} \tag{2}$$

where $\mathbf{X}_k^{\mathrm{CR}}$ is static clutter signal, i.e., $\mathbf{X}_k^{\mathrm{CR}} = \mathbf{r}_{c(k)}[m]$, $\mathbf{Z}_k^{\mathrm{CR}}$ represents the radar scan in scan k, i.e., $\mathbf{Z}_k^{\mathrm{CR}} = \mathbf{r}_{(k)}[m]$, $\mathbf{F} = \mathbf{I}_{m\times m}$, $\mathbf{H} = \mathbf{I}_{m\times m}$, and $\mathbf{I}_{m\times m}$ is an identity matrix. $\mathbf{w}_{k-1}^{\mathrm{CR}}$ and $\mathbf{v}_{\mathrm{k}}^{\mathrm{CR}}$ are the process and measurement noises.

The radar samples with a larger amplitude than that of reflected from various backgrounds should be figured out for extracting target signals. However, the signal strength varies with respect to time in practice. Therefore, an optimal threshold in the amplitude should be used to avoid data loss or miss detection. The threshold can be determined adaptively to the signal using CFAR detection. CFAR detection is a general adaptive algorithm in radar fields to detect the target returns against background noises and clutters in [18]. In particular, Cell Averaging CFAR (CA-CFAR) in [19] is applied to the static clutter reduced signals expressed in (2).

CA-CFAR detection utilizes a sliding window composed of three cells: reference cell (RC), guard cell (GC), and cell under test (CUT), as shown in Fig. 2. The signal processing from each cell can be expressed in (3) to (5). Fig. 3 represents an example of the CA-CFAR processing to the UWB radar measurement. The static clutter reduced signals from (2) are injected as inputs of the CA-CFAR as a blue line. Then the optimal threshold can be calculated as a black line, and the signals which have larger amplitude than the threshold are treated as target measurement candidates.

$$P_n = \frac{1}{2N}\left(\sum_{k=1}^{N} X_k + \sum_{l=N+N_C}^{2N+N_C} X_l\right) \tag{3}$$

$$c_{CFAR} = N\left(P_{FA}^{-1/N} - 1\right) \tag{4}$$

$$\begin{cases} d_1 = 1, & \text{for avg}(X_{CUT}) \geq c_{CFAR}P_n \\ d_1 = 0, & \text{for avg}(X_{CUT}) < c_{CFAR}P_n \end{cases} \tag{5}$$

$$\begin{cases} d_2 = 1, & \text{for } X_{d_1=1} \geq mean(c_{CFAR}P_{(n=1,\cdots,m)}) \\ d_2 = 0, & \text{for } X_{d_1=1} < mean(c_{CFAR}P_{(n=1,\cdots,m)}) \end{cases} \tag{6}$$

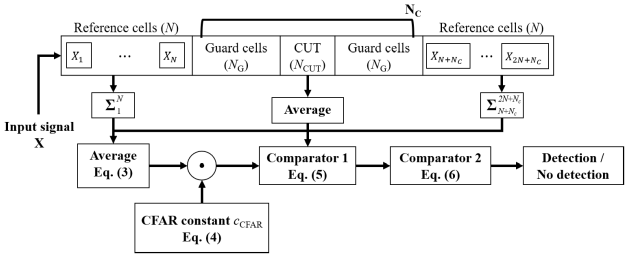

FIGURE 2. Block diagram of CA-CFAR detection.

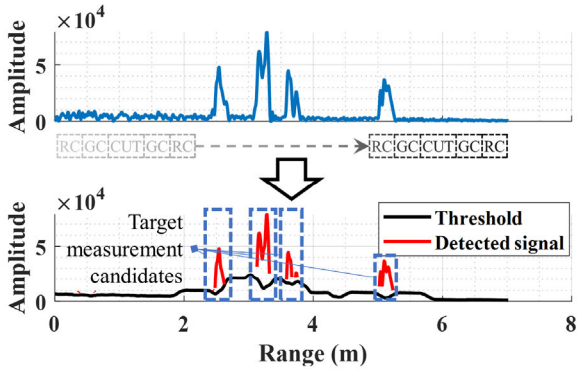

FIGURE 3. CA-CFAR process to UWB radar measurement.

where P_n is the average noise amplitude, N, N_G, and N_{CUT} are the number of samples in RC, GC, and CUT respectively, and N_C is the sum of $2N_G$ and N_{CUT}. The amplitude of signals is denoted by X, P_{FA} is a desired false alarm rate, and d is a Boolean index for detection.

B. MULTIPLE TARGET TRACKING STEP

The radar signal is easily contaminated with moving clutter signals and noise in the target signal candidates in spite of the static clutter reduction and CFAR detection. Moreover, it is difficult to identify the source signal of target and measurement origin. Hence, a data association algorithm should be applied to associate measurements from the moving targets as well as clutter signals. However, if the targets are stationary, the reflected signals from the targets cannot be distinguished in the preprocessing step. Consequently, the target measurement candidates for the MTT cannot be detected, hence the MTT tracker judges there is no target. In addition, if the

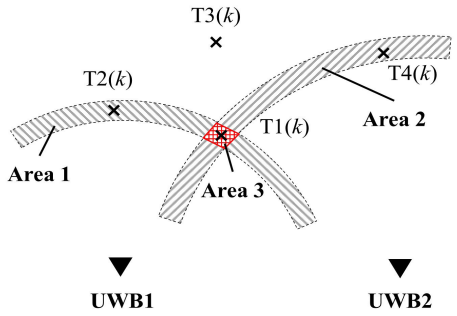

FIGURE 4. Concept of the range- and position-based MTT algorithms.

moving target goes into stationary state, the MTT tracker judges the target tracks become extinct. Therefore, if the stationary target tracking is necessary, it is possible by removing the static clutter reduction method in the preprocessing step with more than three UWB radars.

Fig. 4 illustrates both range-based MTT and position-based MTT. Indeed, the UWB radar provides only the distance measurements, not a bearing angle. Hence, more than two UWB radars are required to track the 2D positions of moving targets. The range-based MTT algorithm based on the LM-IPDA associates the range measurement from each UWB radar individually. Hence, the LM-IPDA is performed as many as the number of UWB radars. For example, the range-based MTT is utilized to track the target 1 (T1) using UWB 1, as shown in Fig. 4. All measurements from targets/clutters within Area 1 are considered as target candidates because the bearing does not provide. In other words, both T1 and T2 are considered as target candidate. It is vulnerable to miss-tracking. On the other hands, the position-based MTT algorithm based on the msLM-IPDA associates the range measurements from all of the UWB radars simultaneously to track the position of targets. Unlike the range-based MTT tracking T1, the measurement from both UWB 1 and 2 are used simultaneously from the targets and clutters within Area 3 (red dashed area) as target candidates. Hence, the position-based MTT algorithm could have robustness against miss-tracking.

1) RANGE-BASED MTT ALGORITHM (LM-IPDA)

The state vector of the range-based MTT algorithm is the distance and its first derivative, $\mathbf{x}_k^\tau = [r_k^\tau, \dot{r}_k^\tau]^T$, where r_k^τ and $\dot{r}_k^\tau$ are the k^{th} distance between the target τ and the UWB radar and its first derivative, respectively, expressed in (7).

$$\mathbf{x}_k^\tau = \mathbf{F}_k \mathbf{x}_{k-1}^\tau + \mathbf{w}_{k-1}, \tag{7}$$

where $\mathbf{F}_k$ is a kinematic propagating model detailed in Table 1, τ indicates the track label as well as target label, w_{k-1} is a process noise which has a white Gaussian and covariance matrix $\mathbf{Q}_{k-1} = q[T^4\mathbf{I}_{2\times2}/4, T^4\mathbf{I}_{2\times2}/2; T^4\mathbf{I}_{2\times2}/2, T^2\mathbf{I}_{2\times2}]$, q is a scaler which represents the acceleration uncertainty in process noise model, and T is a sampling time interval.

The range measurement, $\mathbf{Z}_k^\tau$, is calculated by the propagation delay of target candidates, obtained in (6), multiplied by a speed of light. The measurement model for range-based MTT can be expressed in (8).

TABLE 1. Differences between Range-based and Position-based MTT Algorithms.

	Range-based	Position-based
MTT Algorithm	Multiple LM-IPDA	msLM-IPDA
$\mathbf{x}^\tau_k$	$[r^\tau_k, \dot{r}^\tau_k]^T$	$[x^\tau_k, y^\tau_k, \dot{x}^\tau_k, \dot{y}^\tau_k]^T$
$\mathbf{F}_k$	$\begin{bmatrix} 1 & T \\ 0 & 1 \end{bmatrix}$	$\begin{bmatrix} \mathbf{I}_{2\times2} & T\mathbf{I}_{2\times2} \\ \mathbf{0}_{2\times2} & \mathbf{I}_{2\times2} \end{bmatrix}$
$\mathbf{H}_k$	$\begin{bmatrix} 1 & 0 \end{bmatrix}$	$\begin{bmatrix} \frac{x^\tau_k - x_1}{\lVert \mathbf{x}^\tau_k - \mathbf{x}_1 \rVert} & \frac{y^\tau_k - y_1}{\lVert \mathbf{x}^\tau_k - \mathbf{x}_1 \rVert} & 0 & 0 \\ \vdots & \vdots & \vdots & \vdots \\ \frac{x^\tau_k - x_{m_r}}{\lVert \mathbf{x}^\tau_k - \mathbf{x}_{m_r} \rVert} & \frac{y^\tau_k - y_{m_r}}{\lVert \mathbf{x}^\tau_k - \mathbf{x}_{m_r} \rVert} & 0 & 0 \end{bmatrix}$

$$\mathbf{Z}_k^\tau = \mathbf{H}_k \mathbf{x}_k^\tau + \mathbf{v}_k \tag{8}$$

where $\mathbf{H}_k$ is a measurement matrix in Table 1, and $\mathbf{v}_k$ is a measurement noise which has zero-mean and covariance matrix $\mathbf{R}_k$.

Fig. 5 shows the LM-IPDA algorithm composed of five steps: track initialization, prediction, measurement selection (gating), data association, and update (merging). The tracks are initialized using each pair measurement received from two consecutive scans by a two-point track initialization technique [10].

In prediction, the *a-posteriori* probability density function (pdf) of the target track state $p\{\mathbf{x}_{k-1}^\tau | \chi_{k-1}{}^\tau, \mathbf{Z}_{k-1}\}$, and target existence probability $p\{\chi_{k-1}{}^\tau | \mathbf{Z}_{k-1}\}$ where χ_{k-1} denotes target existence event in k-1 scan are propagated to k scan by the KF propagator in (9), and Markov Chain transition probability α in (10).

$$[\bar{\mathbf{x}}_{k|k-1}^\tau, \bar{\mathbf{P}}_{k|k-1}^\tau] = \mathrm{KF_P}(\hat{\mathbf{x}}_{k-1|k-1}^\tau, \hat{\mathbf{P}}_{k-1|k-1}^\tau, \mathbf{F}_k, \mathbf{Q}_{k-1}) \tag{9}$$

$$p\{\boldsymbol{\chi}_k^\tau | \mathbf{Z}_{k-1}\} = \alpha p\{\boldsymbol{\chi}_{k-1}^\tau | \mathbf{Z}_{k-1}\} \tag{10}$$

where $\bar{\mathbf{x}}_{k|k-1}^\tau, \bar{\mathbf{P}}_{k|k-1}^\tau$ are the *a-priori* state and its covariance in the k^{th} scan. $\hat{\mathbf{x}}_{k-1|k-1}^\tau$ and $\hat{\mathbf{P}}_{k-1|k-1}^\tau$ are the *a-posteriori* state and its covariance in k-1 scan, respectively.

In measurement selection, the measurement set is selected within a probability distance radius of the *a-priori* state not only to reduce the computing load, but also to remove the effect by other targets or clutters. A validation measurement selection criterion in (11) is used to select a subset of measurement $\mathbf{z}_k^\tau$ from (8) with respect to the associated track τ. The validation threshold, σ, is used to specify the validated measurements in the validation gate and can be calculated from the gating probability, P_G in (12).

$$(\mathbf{H}_k \bar{\mathbf{x}}_{k|k-1}^\tau - Z_{k,i})^T \mathbf{S}_{k|k-1}^{-1} (\mathbf{H}_k \bar{\mathbf{x}}_{k|k-1}^\tau - Z_{k,i}) \le \sigma \tag{11a}$$

$$\mathbf{S}_{k|k-1} = \mathbf{H}_k \bar{\mathbf{P}}_{k|k-1}^\tau \mathbf{H}_k^T + \mathbf{R}_k \tag{11b}$$

$$P_G = 1 - e^{-0.5\sigma} \tag{12}$$

where $Z_{k,i}$ denotes the i^{th} measurement in k scan. The measurement likelihood of selected measurement by (11),

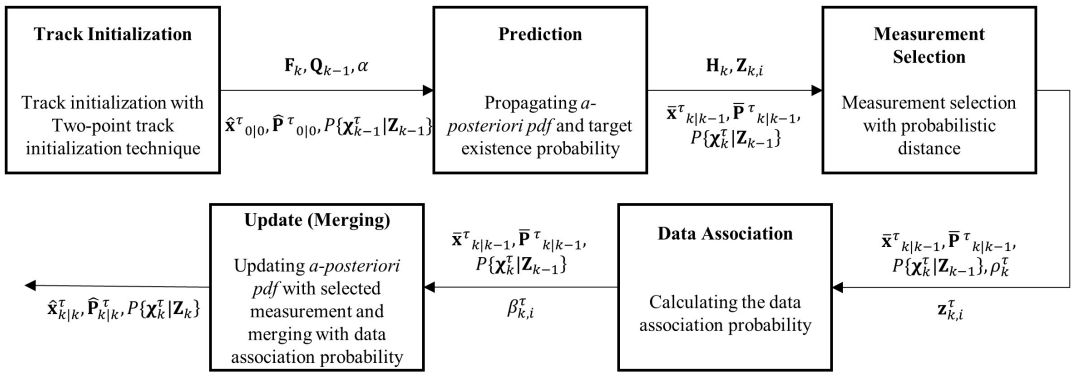

FIGURE 5. Flowchart of LM-IPDA algorithm.

associated with the track τ is calculated in (13). The measurement likelihood of selected measurement by (11), associated with the track τ is calculated in (13).

$$l^{\tau}_{k,i} = p\{\mathbf{z}^{\tau}_{k,i}, \bar{\mathbf{x}}^{\tau}_{k|k-1} | \mathbf{Z}_{k-1}\} = \frac{1}{P_G} N(\mathbf{z}^{\tau}_{k,i}; \mathbf{H}_k \bar{\mathbf{x}}^{\tau}_{k|k-1}, \mathbf{S}_{k|k-1}) \tag{13}$$

where $l_{k,i}{}^{\tau}$ represents the i^{th} measurement likelihood. $\mathbf{z}^{\tau}_{k,i}$ indicates the i^{th} selected measurement.

In the data association step, data association probabilities with respect to each track are firstly calculated by assuming that the measurement $\mathbf{z}^{\tau}_{k,i}$ assigned to track τ is the detection of target τ, and has *a-priori* probability in (14). Secondly, assume that other tracks are following the clutter measurement. Thus, when updating the current track τ based on $\mathbf{z}^{\tau}_{k,i}$, the clutter measurement is modulated with *a-priori* measurement being followed by other tracks that can be subsequently ignored.

$$P^{\tau}_{k,i} = P_D P_G P\{\boldsymbol{\chi}^{\tau}_{k} | \mathbf{Z}_{k-1}\} \frac{l^{\tau}_{k,i}/\rho^{\tau}_{k}}{\sum_{i=1}^{n_k} l^{\tau}_{k,i}/\rho^{\tau}_{k}} \tag{14}$$

where ρ^{τ}_{k} is a clutter measurement density, n_k is the number of the selected measurements, and P_D is the probability of detection. The modulated clutter measurement density $\Omega^{\tau}_{k,i}$ followed by other neighbored track η is expressed in (15).

$$\Omega^{\tau}_{k,i} = \rho^{\tau}_{k} + \sum_{\substack{\eta=1 \\ \eta \neq \tau}}^{\tau_n} \frac{l^{\eta}_{k,i} P^{\eta}_{k,i}}{(1 - P^{\eta}_{k,i})} \tag{15}$$

where τ_n is the number of tracks except τ^{th} track and denominator term in (15) defines the *a-priori* probability that the i^{th} selected measurement associated with tracking η is not originated from the target τ.

In the track update step, the modified clutter measurement density from (15) is used to calculate the track likelihood ratio and the data association probabilities in (16) and (17), respectively.

$$\Lambda^{\tau}_{k} = 1 - P_D P_G + P_D P_G \sum_{i=1}^{n_k} \frac{l^{\tau}_{k,i}}{\Omega^{\tau}_{k,i}} \tag{16}$$

$$\beta^{\tau}_{k,i} = \frac{1}{\Lambda^{\tau}_{k}} \begin{cases} 1 - P_D P_G, & i = 0 \\ P_D P_G \dfrac{l^{\tau}_{k,i}}{\Omega^{\tau}_{k,i}}, & i > 0 \end{cases} \tag{17}$$

The *a-posteriori* probability of target existence is updated using the track likelihood ratio from in (18).

$$P\{\boldsymbol{\chi}^{\tau}_{k} | \mathbf{Z}_{k}\} = \frac{\Lambda^{\eta}_{k} P\{\boldsymbol{\chi}^{\tau}_{k} | \mathbf{Z}_{k-1}\}}{1 - (1 - \Lambda^{\eta}_{k}) P\{\boldsymbol{\chi}^{\tau}_{k} | \mathbf{Z}_{k-1}\}} \tag{18}$$

The *a-posteriori* pdf of target track state, $p\{\mathbf{x}^{\tau}_{k} | \chi^{\tau}_{k}, \mathbf{Z}_{k}\}$ is calculated by the KF estimator, KF_{E}, based on the validated measurement in (19). Each track state estimate and its covariance are merged by using the data association probability as the weighting coefficient in (20) and (21).

$$[\hat{\mathbf{x}}^{\tau}_{k|k,i}, \hat{\mathbf{P}}^{\tau}_{k|k,i}] = \text{KF}_{\text{E}}(\bar{\mathbf{x}}^{\tau}_{k|k-1}, \bar{\mathbf{P}}^{\tau}_{k|k-1}, \mathbf{z}^{\tau}_{k,i}, \mathbf{R}_k) \tag{19}$$

$$\hat{\mathbf{x}}^{\tau}_{k|k} = \sum_{i \geq 0} \beta^{\tau}_{k,i} \hat{\mathbf{x}}^{\tau}_{k|k,i} \tag{20}$$

$$\hat{\mathbf{P}}^{\tau}_{k|k} = \sum_{i \geq 0} \beta^{\eta}_{k,i} [\hat{\mathbf{P}}^{\tau}_{k|k,i} + \hat{\mathbf{x}}^{\tau}_{k|k,i} (\hat{\mathbf{x}}^{\tau}_{k|k,i})^T] - \hat{\mathbf{x}}^{\tau}_{k|k} (\hat{\mathbf{x}}^{\tau}_{k|k})^T \tag{21}$$

Finally, the tracked range from multiple LM-IPDA are gathered in the positioning center to estimate the positions of the targets by using EKF positioning. The state of EKF positioning is the positions and the velocities of targets, $\mathbf{X}^{P}_{k} = [x_k, y_k, \dot{x}_k, \dot{y}_k]^T$, and the measurement is the tracked range data which is the result of LM-IPDA. Hence, the kinematic model and measurement model are the same as the case of the position-based MTT algorithm.

2) POSITION-BASED MTT ALGORITHM (msLM-IPDA)

The state vector of the position-based MTT algorithm is 2D position and velocity, $\mathbf{x}^{\tau}_{k} = [x^{\tau}_{k}, y^{\tau}_{k}, \dot{x}^{\tau}_{k}, \dot{y}^{\tau}_{k}]^T$, expressed in (7) where the kinematic model $\mathbf{F}_k$ is noted in Table 1. Since the relationship between the state and measurement is nonlinear, the nonlinear measurement model $h_{k,j}(\mathbf{x}^{\tau}_{k})$ can be expressed

in (22).

$$\mathbf{Z}_k^\tau = \begin{bmatrix} \mathbf{Z}_{k,i,1}^\tau \\ \vdots \\ \mathbf{Z}_{k,i,m_r}^\tau \end{bmatrix} = \begin{bmatrix} h_{k,1}(\mathbf{x}_k^\tau) \\ \vdots \\ h_{k,m_r}(\mathbf{x}_k^\tau) \end{bmatrix} + \mathbf{v}_k \tag{22}$$

where $h_{k,j}(\mathbf{x}_k^\tau) = \|\mathbf{x}_k^\tau - \mathbf{x}_j\|$, the index j indicates j^{th} UWB radar. m_r is the total number of UWB radars.

In prediction step, target position state and existence probability are propagated to k scan by the EKF based propagator in (23) and (10).

$$[\bar{\mathbf{x}}_{k|k-1}^\tau, \bar{\mathbf{P}}_{k|k-1}^\tau] = \mathrm{EKF_P}(\hat{\mathbf{x}}_{k-1|k-1}^\tau, \hat{\mathbf{P}}_{k-1|k-1}^\tau, \mathbf{F}_k, \mathbf{Q}_{k-1}) \tag{23}$$

The measurement selection step follows the prediction step. Measurements $\mathbf{z}_{k,i,j}^\tau$ within certain probabilistic distance are selected by validation criterion in (24).

$$(h_{k,j}(\bar{\mathbf{x}}_{k|k-1}^\tau) - \mathbf{Z}_{k,i,j})^T \mathbf{S}_{k|k-1}^{-1} (h_{k,j}(\bar{\mathbf{x}}_{k|k-1}^\tau) - \mathbf{Z}_{k,i,j}) \le \sigma \tag{24}$$

where $\mathbf{Z}_{k,i,j}$ denotes the i^{th} measurement received from the j^{th} radar in k scan. Then, the measurement likelihood of $\mathbf{z}_{k,i,j}^\tau$ is calculated in (25).

$$\begin{aligned} l_{k,i,j}^\tau &= p\{\mathbf{z}_{k,i,j}^\tau, \bar{\mathbf{x}}_{k|k-1}^\tau | \mathbf{Z}_{k-1}\} \\ &= \frac{1}{P_G} N(\mathbf{z}_{k,i,j}^\tau; h_k(\bar{\mathbf{x}}_{k|k-1}^\tau), \mathbf{S}_{k|k-1}) \end{aligned} \tag{25}$$

where $l_{k,i,j}^\tau$ represents the i^{th} measurement likelihood from the j^{th} radar. With the measurement likelihood, the modulated clutter measurement density is calculated in (26).

$$\Omega_{k,i,j}^\tau = \rho_k^\tau + \sum_{\substack{\eta=1 \\ \eta \neq \tau}}^{\tau_n} \frac{l_{k,i,j}^\eta P_{k,i,j}^\eta}{(1 - P_{k,i,j}^\eta)} \tag{26}$$

where $P_{k,i,j}^\eta$ is calculated in (14) for the j^{th} UWB radar measurement.

In the data association, track likelihood ratio and data association probabilities are calculated in (27) and (28) using the modified clutter measurement density in (26).

$$\begin{aligned} \Lambda_k^\tau &= \prod_{j=1}^{m_r} \Lambda_{k,j}^\tau \\ &= \prod_{j=1}^{m_r} \left(1 - P_D P_G + P_D P_G \sum_{i=1}^{n_{k,j}} \frac{l_{k,i,j}^\tau}{\Omega_{k,i,j}^\tau} \right) \end{aligned} \tag{27}$$

$$\beta_{k,i,j}^\tau = \frac{1}{\Lambda_k^\tau} \prod_{j:\{i=0\}} (1 - P_D P_G) \prod_{j:\{i\neq 0\}} P_D P_G \frac{l_{k,i,j}^\tau}{\Omega_{k,i,j}^\tau} \tag{28}$$

In the track update step, the *a-posteriori* target existence probability is updated with the track likelihood ratio in (18). The *a-posteriori* pdf of target track state, $p\{\mathbf{x}_k^\tau | \chi_k^\tau, \mathbf{Z}_k\}$ is calculated by the EKF estimator in (29). Then, the target state and its covariance are merged with the data association probability with the weighting coefficient in (30) and (31).

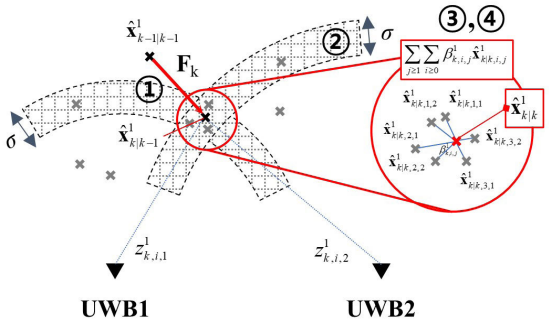

FIGURE 6. Conceptual illustration of the position-based MTT. ①, ②, ③, and ④ indicate the prediction, measurement selection, data association, and track update steps, respectively.

The update step indicates that the objects T1 only within Area 3 are treated as the target as shown in Fig. 4.

$$\begin{aligned} &[\hat{\mathbf{x}}_{k|k,i,j}^\tau, \hat{\mathbf{P}}_{k|k,i,j}^\tau] \\ &\quad = \mathrm{EKF_E}(\bar{\mathbf{x}}_{k|k-1}^\tau, \bar{\mathbf{P}}_{k|k-1}^\tau, \{\mathbf{z}_{k,i,1}^\tau, \cdots, \mathbf{z}_{k,i,m_r}^\tau\}, \mathbf{R}_k) \end{aligned} \tag{29}$$

$$\hat{\mathbf{x}}_{k|k}^\tau = \sum_{j\ge 1} \sum_{i\ge 0} \beta_{k,i,j}^\tau \hat{\mathbf{x}}_{k|k,i,j}^\tau \tag{30}$$

$$\begin{aligned} \hat{\mathbf{P}}_{k|k}^\tau = &\sum_{j\ge 1} \sum_{i\ge 0} \beta_{k,i,j}^\eta [\hat{\mathbf{P}}_{k|k,i,j}^\tau + \hat{\mathbf{x}}_{k|k,i,j}^\tau (\hat{\mathbf{x}}_{k|k,i,j}^\tau)^T] \\ &- \hat{\mathbf{x}}_{k|k}^\tau (\hat{\mathbf{x}}_{k|k}^\tau)^T \end{aligned} \tag{31}$$

The msLM-IPDA follows the same procedure as the LM-IPDA, but they have two main differences due to different state vectors and linearity between the position vectors in the msLM-IPDA and the distance vectors in the LM-IPDA. First, the EKF as (23) and (29) in the msLM-IPDA is utilized rather than the KF as (9) and (19) in the LM-IPDA. Second, the msLM-IPDA computes the probability for measurements from all UWB radars simultaneously in (25) ∼ (31) while the LM-IPDA computes the probability for measurements from each UWB radar separately in (13) ∼ (21). The conceptual illustration of the msLM-IPDA is demonstrated in Fig. 6.

III. NUMERICAL SIMULATION

Numerical simulations are evaluated to verify the performance of the MTT system. Firstly, tracking performance is performed with the dilution of precision (DOP) to validate the accuracy with respect to the UWB radar placement. The second simulation is performed to investigate the performance of the MTT algorithms.

The DOP is a term used in the Global Positioning System (GPS) to specify the position error as a mathematical effect of satellite geometry on the accuracy of position measurement [20]. The DOP value can be interpreted as the output position error over the measured range error, as shown in (32), (33), and (34).

$$\mathbf{A} = \begin{bmatrix} (x - x_1)/r_1 & (y - y_1)/r_1 \\ (x - x_2)/r_2 & (y - y_2)/r_2 \end{bmatrix} \tag{32}$$

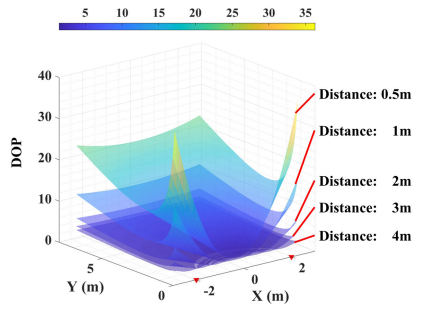

FIGURE 7. DOP regarding distances between UWB radars.

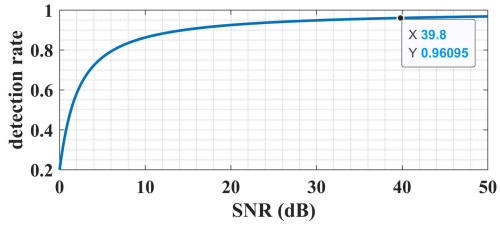

FIGURE 8. Detection rate of the CA-CFAR.

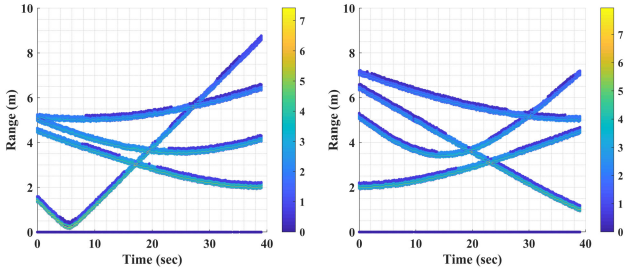

FIGURE 9. Results of CA-CFAR detection in whole scans. (a) and (b) are from UWB radar 1 and 2, respectively.

$$\mathbf{Q}_{dop} = (\mathbf{A}^T\mathbf{A})^{-1} = \begin{bmatrix} \sigma_x^2 & \sigma_{xy} \\ \sigma_{xy} & \sigma_y^2 \end{bmatrix} \tag{33}$$

$$HDOP = \sqrt{\sigma_x^2 + \sigma_y^2} \tag{34}$$

where x_j and y_j are the positions of j^{th} UWB radar module, $HDOP$ is the horizontal DOP, which indicates 2D position accuracy. The larger DOP means the worse position accuracy. In the simulation, the distance between two UWB radars varies from 0.5 meters to 4 meters to verify the effect of the distance on the position accuracy. As shown in Fig. 7, DOP value increases as the distance decreases, and the distance is set as 4 meters.

The range measurement between two UWB radars and trajectories of four targets includes 0.05 meters level of Gaussian random noise. Then, CA-CFAR detection algorithm is applied to determine the threshold of measured signals. The detection rate of the CA-CFAR detection regarding to the signal-to-noise ratio (SNR) is demonstrated in Fig. 8. The SNR of the input signals of the CFAR is about 40dB, hence the detection rate is about 0.9. The result of the CA-CFAR detection in whole scans are shown in Fig. 9.

TABLE 2. Parameters of CA-CFAR Detection and MTT Algorithm.

CA-CFAR Detection Parameters	
Number of RC	80
Number of GC	20
Number of CUT	2
Desired false alarm rate	0.2
MTT Algorithm Parameters	
Time interval (T)	0.2 s
Detection probability (P_D)	0.9
Clutter measurement density ($\rho_{k,i}^{\eta}$)	1e-4
Gating threshold (σ)	3

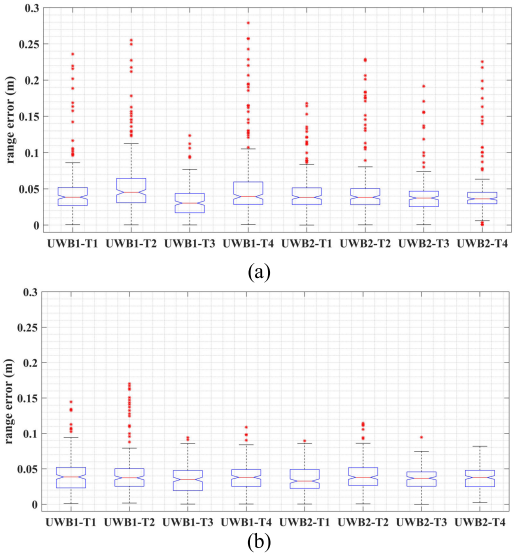

FIGURE 10. Tracked range error statistics. (a) is the result of range-based MTT (LM-IPDA) and (b) is the result of position-based MTT (msLM-IPDA).

The desired parameters for the CA-CFAR in (2)-(4) and the target tracking algorithm are specified in Table 2. The tracking performance of the position-based MTT is compared with the range-based MTT. Fig. 10 represents the error statistics of the tracked range. Both algorithms can track the multiple targets without miss tracking. However, the range-based MTT shows large peak errors, and the phenomena frequently occur when the measurements are crossing each other.

Fig. 11(a) is the 2D position tracking results of the position and range-based MTT. The simulation has been performed 100 times. Even if trajectories of four targets are crossed each other, the position-based MTT can track the multiple targets with more accurate and robust against clutter environment than the range-based MTT. Fig. 11(b) and Table 3 represent the statistical results of the position root mean square error (RMSE) of each algorithm. As the result shows, the position-based MTT can track the multiple targets with more accurate and robust against clutter environments than the range-based MTT.

IV. EXPERIMENTAL ANALYSIS

Tracking and positioning performance of both MTT algorithms with UWB radars are experimentally investigated in an 8m×6m indoor area with moving targets (humans) similar

TABLE 3. 2D position error of the simulation.

Unit: meter	Position-based MTT (msLM-IPDA)			
	Target 1	Target 2	Target 3	Target 4
RMSE (STD)	0.0775 (0.0666)	0.0836 (0.0458)	0.0774 (0.0299)	0.0708 (0.0714)
Peak error	0.1667	0.2227	0.1442	0.2590
Unit: meter	Range-based MTT (LM-IPDA)			
	Target 1	Target 2	Target 3	Target 4
RMSE (STD)	0.1067 (0.0778)	0.1093 (0.0605)	0.0792 (0.0228)	0.1109 (0.0870)
Peak error	0.4279	0.3632	0.1721	0.4398

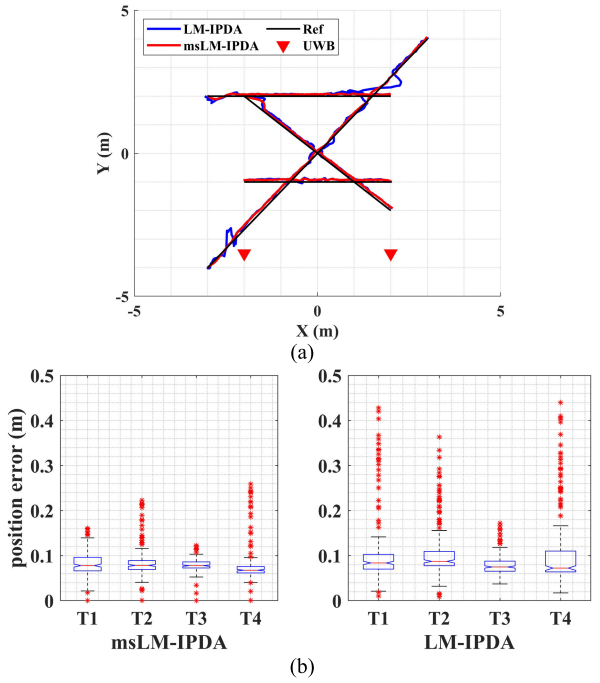

FIGURE 11. 2D position tracking simulation result. (a) is the 2D position tracking result by position-based MTT and range-based MTT. (b) is the box plot for 2D position RMSE.

to the numerical simulation. The targets are initially separated but moving along the cross trajectories. A motion capture system is utilized to measure the reference tracking position. The parameters of MTT algorithms are the same as the parameters of simulation in Table 2.

Two Time Domain P440 UWB radars are used in bistatic mode and separately placed with a distance of about 4 meters, same as the DOP simulation in Fig. 6. Each UWB radar has two BroadSpec antennas, one is for transmitting and the other is for receiving the reflected signals from targets. The two UWB radars are connected to a WLAN to control the radars by using a control software through an UDP network. Table 4 is the brief specifications and settings of the UWB radar and antenna used for the experiment. Reflected signals from both moving targets and clutters are measured by UWB radar modules, and the target candidates are selected through the preprocessing algorithm.

In the experimental analysis, two scenarios are considered: scenario 1 is to track two moving targets in environment

TABLE 4. UWB radar specifications.

Time Domain's P440 UWB Radar	
Operating Band (Center frequency)	3.1 GHz~4.8 GHz (4.3 GHz)
RF Bandwidth	1.61 GHz
Maximum power spectral density	-41 dBm/MHz
Sampling rate	5 Hz
Time Domain's BroadSpec Antenna	
Radiated Waveform	500ps Monocycle:1ns Waveform
Pattern	Omni in azimuth to ±1.5dB
Polarization	Vertical
VSWR (voltage standing wave ratio)	~1.75:1
Gain	Nominally ~3dBi

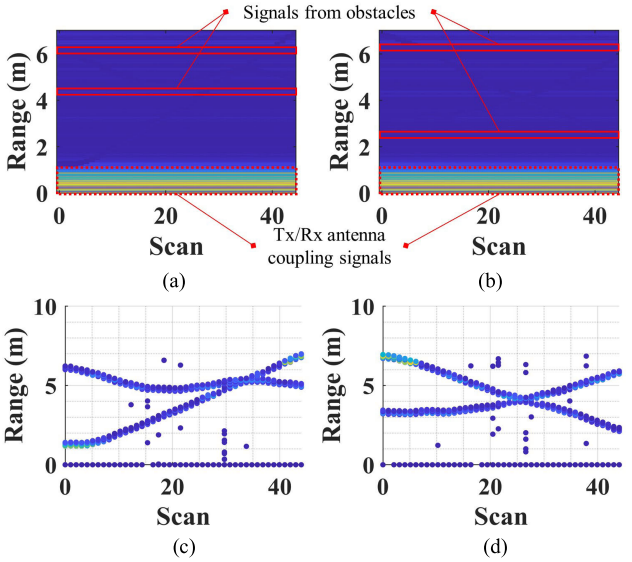

FIGURE 12. (a) and (b) are the raw reflected signals in whole scans, measured by two UWB radars, respectively. (c) and (d) are the results of the preprocessing algorithm.

including two obstacles and static clutters around the test area; scenario 2 is to track four moving targets in environment including static clutters. The tracking performances of the position-based MTT are compared with the range-based MTT, the global nearest neighbor (GNN) algorithm [22], and track oriented multiple hypothesis tracking (TO-MHT) [23].

A. SCENARIO 1

Fig. 12 shows the raw signals and the results of the preprocessing algorithm in whole scans. The raw signals in Figs. 12(a) and (b) include the antenna coupling signals between transmitting and receiving antennas, reflected signals from targets, clutters, and obstacles. Figs 12(c) and (d) show the results of the preprocessing algorithm. The preprocessing algorithm can provide the distance measurements of moving targets with some noise signals which are treated as clutters in tracking algorithm.

Fig. 13 shows the tracking results of each method. The GNN and the LM-IPDA have miss-tracking points, resulting in large position errors. On the contrary, the msLM-IPDA and the TOMHT can track the two targets without miss-tracking,

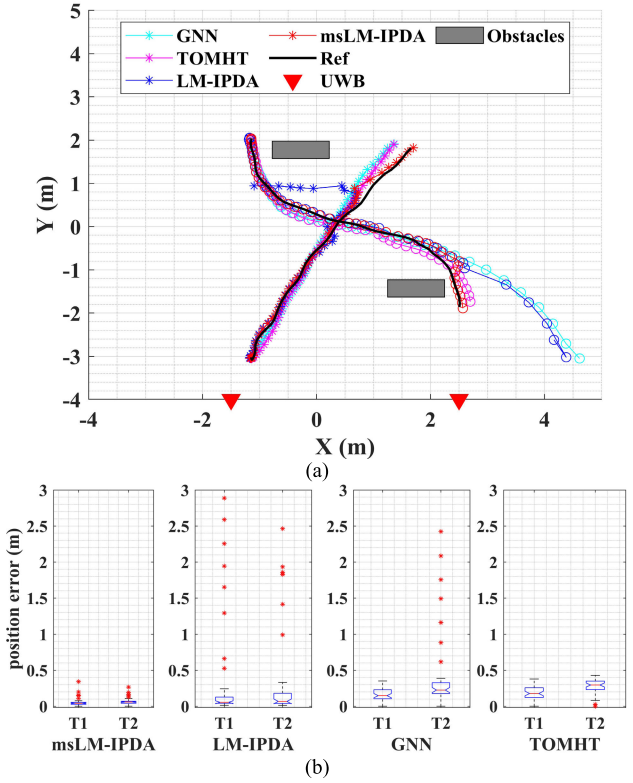

FIGURE 13. 2D position tracking experimental result for two targets. (a) is the 2D position tracking results by msLM-IPDA, LM-IPDA, GNN and TOMHT. Star (∗) and circle (o) points illustrate target 1 and target 2, respectively. (b) is the box plot for 2D position RMSE.

TABLE 5. 2D position tracking error of scenario 1.

Unit: meter	msLM-IPDA		LM-IPDA	
	Target 1	Target 2	Target 1	Target 2
RMSE	0.0561	0.0677	0.3742	0.3559
(STD)	(0.0580)	(0.0476)	(0.7434)	(0.6531)
Peak error	0.3409	0.2659	2.8879	2.4624
Unit: meter	GNN		TOMHT	
	Target 1	Target 2	Target 1	Target 2
RMSE	0.1700	0.4229	0.1842	0.2878
(STD)	(0.0931)	(0.5398)	(0.0925)	(0.0841)
Peak error	0.3503	2.4227	0.3775	0.4275

but the msLM-IPDA is more accurate than the TOMHT. Fig. 13(b) and Table 5 represent the position RMSE statistics. The msLM-IPDA can track the multiple targets with less than 10 centimeters of mean error.

B. SCENARIO 2

Fig. 14 shows the results of the preprocessing algorithm in the 51st scan from UWB radar 1. Fig. 14(a) shows the raw reflected signals, and the KF static clutter reduction method in (2) removes the static clutter signals and detects the moving targets/clutters signals, as shown in Fig. 14(b). Fig. 14(c) shows the result of the CA-CFAR detection in (3) to (6) where black line is the envelop data; red line is the thresholds in each window; and blue circles are the selected target signal candidates. Consequently, Fig. 15 shows the raw

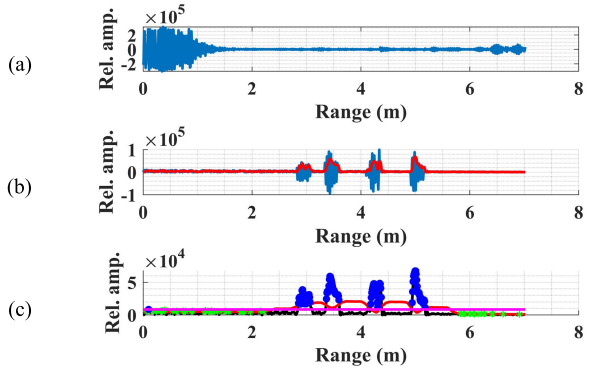

FIGURE 14. Example of 51st scan in UWB 1. (a) raw received signal. (b) static clutter reduced signal (red line is the upper envelop of blue line). (c) results of CA-CFAR detection.

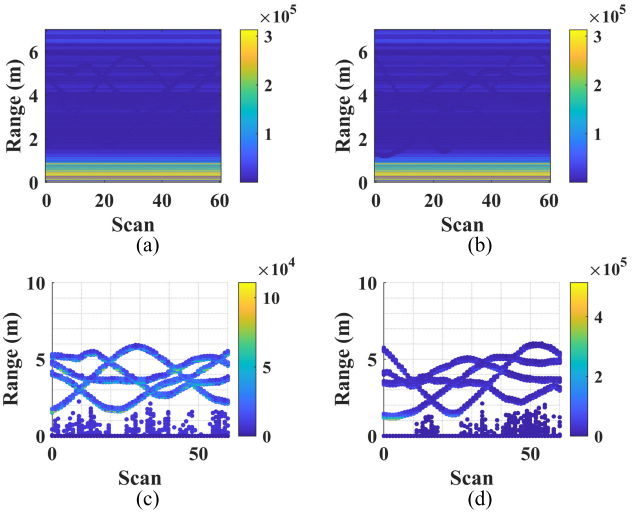

FIGURE 15. (a) and (b) are the raw reflected signals in whole scans, measured by two UWB radars, respectively. (c) and (d) are the results of CA-CFAR detection from two UWB radars. Color bars beside each plot represent the reflected signal strength in a relative level to transmitted signals.

reflected signals and the target signal candidates in whole scans.

As shown in Figs. 15(c) and (d), there are lots of crossing points between each target and clutters. Therefore, the MTT algorithms are applied to track the target positions using the measured range data in the cluttered environments. The tracked positions are compared with the reference positions to verify the accuracy of the proposed system, as shown in Fig. 16 and Table 6. Similar to the scenario 1, the tracking performance of the position-based MTT is compared with the range-based MTT, GNN, and TOMHT.

Fig. 16(a) represents the 2D position tracking experimental results by the msLM-IPDA, the LM-IPDA, GNN, and TOMHT, respectively. In case of the GNN and the LM-IPDA, there are several miss-tracking points because the algorithms miss-track the distance between the targets and the UWB radars. On the other hands, the msLM-IPDA and the TOMHT can track the multiple targets with reasonable performance. However, the TOMHT miss-tracks the target 4.

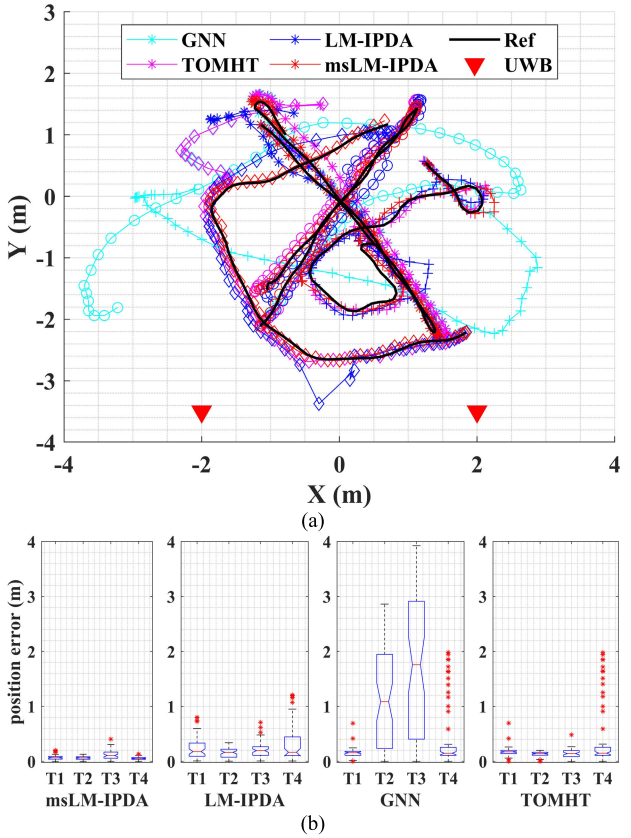

FIGURE 16. 2D position tracking experimental result for four targets. (a) is the 2D position tracking result by msLM-IPDA, LM-IPDA, GNN and TOMHT. Star (∗), circle (o), plus (+), and diamond (◇) points illustrate target 1, 2, 3, and 4, respectively. (b) is the box plot for the 2D position RMSE.

TABLE 6. 2D position tracking error of scenario 2.

Unit: meter	msLM-IPDA			
	Target 1	Target 2	Target 3	Target 4
RMSE	0.0705	0.0627	0.1259	0.0561
(STD)	(0.0392)	(0.0302)	(0.0824)	(0.0267)
Peak error	0.1993	0.1297	0.4042	0.1312
Unit: meter	LM-IPDA			
	Target 1	Target 2	Target 3	Target 4
RMSE	0.2409	0.1584	0.2221	0.3343
(STD)	(0.2010)	(0.0827)	(0.1393)	(0.3488)
Peak error	0.8002	0.3378	0.7090	1.2058
Unit: meter	GNN			
	Target 1	Target 2	Target 3	Target 4
RMSE	0.1567	1.2060	1.8168	0.4476
(STD)	(0.0933)	(0.9384)	(1.2920)	(0.6058)
Peak error	0.6937	2.8617	3.9243	1.9823
Unit: meter	TOMHT			
	Target 1	Target 2	Target 3	Target 4
RMSE	0.1792	0.1358	0.1443	0.4464
(STD)	(0.0901)	(0.0378)	(0.0800)	(0.6070)
Peak error	0.6946	0.1995	0.4821	1.9791

Fig. 16(b) shows the statistical results for performance validation. The RMSE of each target are less than 0.2 meters, and the standard deviations are less than 0.1 meters in case of the position-based MTT. The result shows that the position-based MTT is the most accurate and robust MTT algorithm among the compared MTT techniques.

TABLE 7. Success rate of target tracking algorithms.

Success rate (%)	msLM-IPDA	LMIPDA	GNN	TOMHT
Scenario 1	98.89	81.82	78.41	92.05
Scenario 2	98.75	71.25	55.00	91.25

As a result, the success rates of each tracking algorithm are identified in Table 7. The position-based MTT can track the multiple moving targets with the largest success rate among all tracking algorithms.

V. CONCLUSION

There are several challenges for multiple moving target tracking using multi-static UWB radar system such as clutter signals from undesired sources, and unknown number and behavior of multiple moving targets. This paper proposed a multiple moving target tracking algorithm which includes preprocessing step and MTT step. Preprocessing step which includes static clutter reduction and CFAR detection is applied to extract the target candidate range measurements. For MTT step, this paper investigated the tracking performances of the range-based and position-based MTT algorithms. For the range-based MTT, multiple LM-IPDA are used for tracking range between targets and each UWB radar, then the tracked ranges from each LM-IPDA are utilized to estimate positions of targets in the positioning center. For the position-based MTT, on the other hands, this paper proposed msLM-IPDA for robust and accurate tracking. Numerical simulations and experimental analyses are carried out to verify the multi-target tracking performance of two approaches. In addition, the comparative analyses are investigated with two other tracking algorithms: GNN and TOMHT. Two UWB radar modules are used for transreceiver operation and placed at various distances. The position tracking results are compared with the trajectories from motion capture system. The msLM-IPDA shows accurate and robust performance in noisy environments. The UWB radar system has less than 0.2 meters of position tracking errors without any miss detection even if the trajectories of multiple targets are crossing each other. The proposed algorithm can be applied not only the UWB radar system, but also other multi-static passive radar systems such as a sonar system.

REFERENCES

[1] N. Patwari, J. N. Ash, S. Kyperountas, A. O. Hero, R. L. Moses, and N. S. Correal, "Locating the nodes: Cooperative localization in wireless sensor networks," *IEEE Signal Process. Mag.*, vol. 22, no. 4, pp. 54–69, Jul. 2005.

[2] M. Chiani, A. Giorgetti, and E. Paolini, "Sensor radar for object tracking," *Proc. IEEE*, vol. 106, no. 6, pp. 1022–1041, Jun. 2018.

[3] D. Dardari, A. Conti, U. Ferner, A. Giorgetti, and M. Z. Win, "Ranging with ultrawide bandwidth signals in multipath environments," *Proc. IEEE*, vol. 97, no. 2, pp. 404–426, Feb. 2009.

[4] R. J. Fontana, "Recent system applications of short-pulse ultra-wideband (UWB) technology," *IEEE Trans. Microw. Theory Techn.*, vol. 52, no. 9, pp. 2087–2104, Sep. 2004.

[5] K. Wang, Z. Zeng, and J. Sun, "Through-wall detection of the moving paths and vital signs of human beings," *IEEE Geosci. Remote Sens. Lett.*, vol. 16, no. 5, pp. 717–721, May 2019.

[6] A. Kumar, Z. Li, Q. Liang, B. Zhang, and X. Wu, "Experimental study of through-wall human detection using ultra wideband radar sensors," *Measurement*, vol. 47, pp. 869–879, Jan. 2014.
[7] A. Buonanno, M. D'Urso, G. Prisco, M. Felaco, L. Angrisani, M. Ascione, R. Schiano Lo Moriello, and N. Pasquino, "A new measurement method for through-the-wall detection and tracking of moving targets," *Measurement*, vol. 46, no. 6, pp. 1834–1848, Jul. 2013.
[8] S. Ahmed, F. Khan, A. Ghaffar, F. Hussain, and S. Cho, "Finger-counting-based gesture recognition within cars using impulse radar with convolutional neural network," *Sensors*, vol. 19, no. 6, p. 1429, Mar. 2019.
[9] Y. Bar-Shalom and E. Tse, "Tracking in a cluttered environment with probabilistic data association," *Automatica*, vol. 11, no. 5, pp. 451–460, Sep. 1975.
[10] D. Musicki, R. Evans, and S. Stankovic, "Integrated probabilistic data association," *IEEE Trans. Autom. Control*, vol. 39, no. 6, pp. 1237–1241, Jun. 1994.
[11] T. Fortmann, Y. Bar-Shalom, and M. Scheffe, "Sonar tracking of multiple targets using joint probabilistic data association," *IEEE J. Ocean. Eng.*, vol. 8, no. 3, pp. 173–184, Jul. 1983.
[12] D. Musicki and R. Evans, "Joint integrated probabilistic data association: JIPDA," *IEEE Trans. Aerosp. Electron. Syst.*, vol. 40, no. 3, pp. 1093–1099, Jul. 2004.
[13] S. Challa, R. Evans, M. Morelande, and D. Musicki, "Practical object tracking," in *Fundamentals Object Tracking*. Cambridge, U.K.: Cambridge Univ. Press, 2011, pp. 312–343.
[14] V. H. Nguyen and J. Y. Pyun, "Location detection and tracking of moving targets by a 2D IR-UWB radar system," *Sensors*, vol. 15, no. 3, pp. 6740–6762, 2015.
[15] C. Kim and J.-Y. Lee, "ToA-based multi-target localization and respiration detection using UWB radars," *EURASIP J. Wireless Commun. Netw.*, vol. 2014, no. 1, p. 145, 2014.
[16] C. Kim, J.-Y. Lee, T. Cho, D. Ki, B. H. Cho, and J. Yoon, "Multi-target localization of breathing humans," in *Proc. IEEE Int. Conf. Ultra-Wideband (ICUWB)*, Sep. 2013, pp. 49–54.
[17] B. Gulmezoglu, M. Burak Guldogan, and S. Gezici, "Multiperson tracking with a network of ultrawideband radar sensors based on Gaussian mixture PHD filters," *IEEE Sensors J.*, vol. 15, no. 4, pp. 2227–2237, Apr. 2015.
[18] M. Barkat, S. D. Himonas, and P. K. Varshney, "CFAR detection for multiple target situations," *IEE Proc. F Radar Signal Process.*, vol. 136, no. 5, pp. 193–209, Oct. 1989.
[19] F. D. Almeida Garcia, A. C. Flores Rodriguez, G. Fraidenraich, and J. C. S. Santos Filho, "CA-CFAR detection performance in homogeneous weibull clutter," *IEEE Geosci. Remote Sens. Lett.*, vol. 16, no. 6, pp. 887–891, Jun. 2019.
[20] R. B. Langley, "Dilution of precision," *GPS World*, vol. 10, no. 5, pp. 52–59, 1999.
[21] X. Li, C. Zhao, X. Lu, and W. Wei, "Underwater bearings-only multitarget tracking based on modified PMHT in dense-cluttered environment," *IEEE Access*, vol. 7, pp. 93678–93689, Jul. 2019.
[22] H. Leung, Z. Hu, and M. Blanchette, "Evaluation of multiple radar target trackers in stressful environments," *IEEE Trans. Aerosp. Electron. Syst.*, vol. 35, no. 2, pp. 663–674, Apr. 1999.
[23] S. S. Blackman, "Multiple hypothesis tracking for multiple target tracking," *IEEE Aerosp. Electron. Syst. Mag.*, vol. 19, no. 1, pp. 5–18, Jan. 2004.

MINHO SHIN received the B.E. degree from the School of Mechanical, Aerospace and Nuclear Engineering, Ulsan National Institute of Science and Technology, Ulsan, South Korea, in 2011, where he is currently pursuing the joint M.S. and Ph.D. degree. His current research interests include mechatronics, navigation sensor and positioning, and sensor fusion and control.

HUNGSUN SON (Member, IEEE) received the M.S. degree in aero and astronautical engineering from Stanford University, Stanford, CA, USA, in 2002, and the Ph.D. degree in mechanical engineering from the Georgia Institute of Technology, Atlanta, GA, USA, in 2007. He is currently an Associate Professor in mechanical, aerospace and nuclear engineering with the Ulsan National Institute of Science and Technology (UNIST), South Korea. His current research interests include mechatronics, sensors and actuators, dynamic system modeling, design optimization, automation, and control.